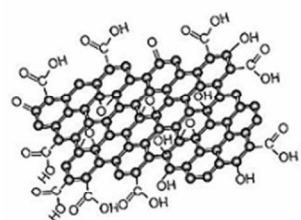


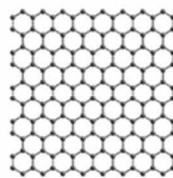
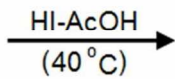


**Performance evaluation of highly conductive graphene (RGOHI-AcOH) and graphene/metal nanoparticle composite (RGO/Ni) coated on carbon cloth for supercapacitor applications**

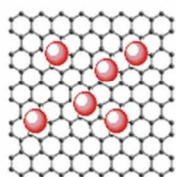
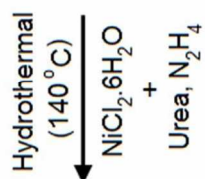
Journal:	<i>RSC Advances</i>
Manuscript ID	RA-ART-07-2015-014806.R2
Article Type:	Paper
Date Submitted by the Author:	13-Oct-2015
Complete List of Authors:	Valipour, Alireza; Yeungnam University, Civil Engineering Hamnabard, Nazanin; Yeungnam University, Mechanical Engineering Ahn, Youngho; Yeungnam University, Civil and environmental Engineering
Subject area & keyword:	Nanomaterials - Materials < Materials



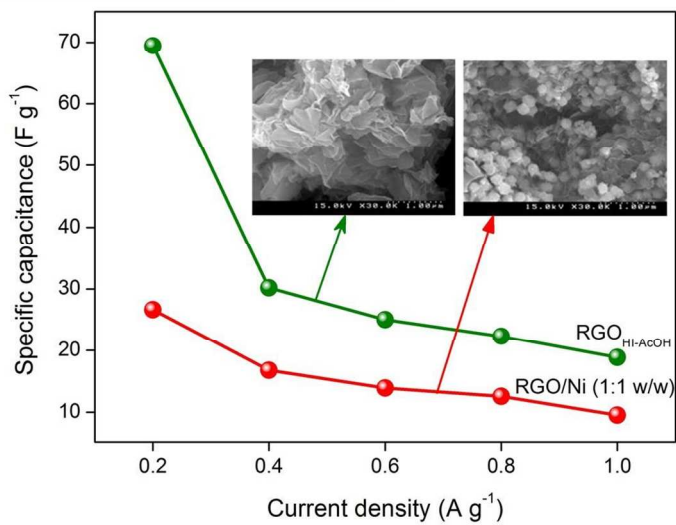
Graphene oxide



Graphene



RGO/Ni nanoparticle composite



247x190mm (150 x 150 DPI)

**Performance evaluation of highly conductive graphene (RGO<sub>HI-AcOH</sub>) and graphene/metal nanoparticle composite (RGO/Ni) coated on carbon cloth for supercapacitor applications**

**Alireza Valipour,<sup>a</sup> Nazanin Hamnabard<sup>b</sup> and Young-Ho Ahn<sup>\*a</sup>**

*<sup>a</sup> Department of Civil Engineering, Yeungnam University, Gyungsan 712-749, South Korea.*

*E-mail: yhahn@ynu.ac.kr; Tel.: +82 53 8103511*

*<sup>b</sup> School of Mechanical Engineering, Yeungnam University, Gyeongsan 712-749 South Korea*

## Abstract

The application of graphene (RGO)-based composites as electrode materials in supercapacitors can be limited by the fabrication complicity and costs, and the non-environmentally friendly nature of the production process. This study examined the effectiveness of high conductive graphene material ( $\text{RGO}_{\text{HI-AcOH}}$ ) compared to produced-hydrazine RGO and graphene nanoparticles composite (RGO/Ni) materials on a carbon cloth substrate in supercapacitors. The composites were synthesized at different mass ratios (as 1:1, 2:1, 4:1, 10:1 and 1:2) of RGO to Ni nanoparticles. All synthesized samples were characterized by X-ray diffraction, scanning electron microscopy, atomic force microscopy, X-ray photoelectron spectroscopy and raman spectroscopy. Methylene blue method was used for determining the specific surface area. The  $\text{RGO}_{\text{HI-AcOH}}$  electrode exhibited higher electrochemical performance ( $40 \text{ F g}^{-1}$  at  $10 \text{ mV s}^{-1}$  and  $70 \text{ F g}^{-1}$  at  $0.2 \text{ A g}^{-1}$ ) and stability ( $\sim 94\%$ ) than the other electrodes examined. Among the prepared composites, the composite with a RGO to Ni nanoparticle mass ratio of 1:1 showed better electrochemical performance ( $30 \text{ F g}^{-1}$  at  $10 \text{ mV s}^{-1}$ , and  $27 \text{ F g}^{-1}$  at  $0.2 \text{ A g}^{-1}$ ) than those of produced-hydrazine RGO and the other composite electrodes. Overall,  $\text{RGO}_{\text{HI-AcOH}}$  as a first priority electrode material (particularly, coated on a carbon cloth substrate) has potential applications in energy storage devices.

**Keywords:** graphene, nickel nanoparticle, composite, carbon cloth, electrochemical performance, supercapacitor

## 1. Introduction

Supercapacitors, as electrochemical energy storage and conversion devices, have attracted considerable interest in recent years owing to their long cycle life (>100000 cycles) and rapid charging and discharging rate at high power densities.<sup>1</sup> Generally, the design and synthesis of low-cost high-performance electrode materials are the key research concept in supercapacitors. Graphene (a two-dimensional giant molecule of sp<sup>2</sup>-bonded carbon atoms) has a theoretical high surface area, high electrical conductivity, good chemical stability, and high mechanical strength, making it a suitable candidate material for supercapacitor electrodes, particularly for electrochemical double-layer capacitors (EDLC).<sup>2</sup> Graphene with an exfoliated structure and good electrical conductivity would be an ideal electrode material for use in energy storage devices.<sup>3</sup> In fact, different graphene production methods results in different types of the same material with a range of electrochemical properties.<sup>4</sup> The preparation of graphene (i.e. reduced graphene oxide, RGO) from the chemical reduction of graphene oxide (GO) is considered one of the most efficient methods for low-cost and large-scale production.<sup>5</sup> When a strong reducing agent (generally hydrazine) is applied, graphene normally suffers from serious aggregation or restacking during the drying process due to van der Waals interactions, which leads to a loss of its electrochemical properties.<sup>2,6</sup> Therefore, one effective solution to prevent aggregation is to incorporate pseudo-capacitive materials (such as RuO<sub>2</sub>, ZnO, NiO, Ni(OH)<sub>2</sub>, TiO<sub>2</sub>, NiCPNP, Ni<sub>x</sub>Co<sub>100-x</sub> etc.) in the graphene nanosheets to maintain their separation, and fully use the advantages of the pseudocapacitor and graphene-based EDLC electrodes.<sup>3,7-11</sup> Ni-nanoparticles would be particularly interesting, owing to their low cost and abundant availability, while the application of RGO/Ni nanoparticle composites has rarely been studied in supercapacitors.

On the other hand, nanocomposite fabrication is complicated and expensive, and might

be non-environmentally friendly due to the toxic nature of the pseudocapacitive materials, which has limited its practical applications on large scale. Despite this, it is important to study RGO/Ni nanoparticle composites for supercapacitors. Moreover, the use of single highly conductive graphene materials can be a practical way of overcoming the limitations associated with graphene nanocomposite materials and increasing the supercapacitor efficiency. For example, Yu et al.<sup>12</sup> demonstrated the electrochemical synthesis of RGO for the electric double-layer capacitors. Sun et al.<sup>13</sup> prepared a RGO paper by a flame-induced reduction of GO paper under ambient conditions. Wang et al.<sup>14</sup> fabricated three dimensional macroporous graphene architectures by a simple template-directed method using polystyrene microspheres. RGO-coated hollow mesoporous carbon spheres are synthesized by a simple template-directed method using phenolic polymer coated polystyrene spheres as templates.<sup>15</sup> Hereupon, hydriodic acid with acetic acid (HI-AcOH) could also be considered as an effective, non-toxic and versatile reducing agent for RGO preparations with high electrical conductivity. While hydrazine reduction of graphene oxide and the decoration of the graphene surface with pseudo-capacitive materials lead to conformational constraints. Therefore, it is important to evaluate the RGO<sub>HI-AcOH</sub> to improve the performance of supercapacitor electrodes. This idea could open up a new opportunity to store energy with high efficiency in supercapacitors. In addition, many efforts have been made to use metallic and glass substrates (such as Ni foam, FTO, ITO, etc.) for loading nanostructure materials.<sup>11, 16-18</sup> A metallic substrate with higher porosity and nano-sized feature is more favorable.<sup>17</sup> Nevertheless, the use of these substrates has several drawbacks, such as high cost and limited supply, fragility and difficult manageability.<sup>16, 18</sup> On the other hand, carbon cloth, which has been used widely as a gas diffusion layer in fuel cells<sup>19</sup>, would also be an attractive alternative electrode support for deposition. Compared to other substrates, carbon cloth is a

very strong, thin, flexible, and lightweight synthetic matrix with high porosity and good electrical conductivity, which could offer a significant advantage for supercapacitor applications. However, carbon cloth has a low surface area due to the large size of carbon fibers ( $\sim 10 \mu\text{m}$ ) and gaps between fibers (*ca.* micro-size) that may limit the area-normalized capacitance.<sup>20,21</sup>

This study examined the feasibility of using high conductive graphene material (RGO<sub>HI-AcOH</sub>) rather than a graphene nanoparticle composite (RGO/Ni) for electrochemical energy storage devices. In particular, RGO/Ni nanoparticle composites at different mass ratios were prepared by a one-step hydrothermal process using hydrazine hydrate as a reducing agent. This can be a practical rationale for determining the synergistic effect between conventionally grown graphene and nanoparticles. Accordingly, RGO was also fabricated without a nanoparticle infusion for comparison. The electrochemical behavior of RGO<sub>HI-AcOH</sub>, as well as hydrazine-produced RGO and RGO/Ni nanoparticle composite-coated carbon cloth substrate was compared to identify the most efficient electrode for supercapacitor applications.

## 2. Experimental methods

### 2.1 Materials

Graphite powder (99.9%) was purchased from Kanto Chemical Co. Inc., Japan. Hydrogen peroxide (H<sub>2</sub>O<sub>2</sub>, 30%) was obtained from Daejung Chemicals & Metals Co., Ltd., Korea. Acetic acid (CH<sub>3</sub>COOH, 99.5%), nickel chloride (NiCl<sub>2</sub>·6H<sub>2</sub>O, 97%), and sodium bicarbonate (NaHCO<sub>3</sub>, 99.5%) were supplied by DC Chemical Co., Ltd., Korea. Hydriodic acid (HI, 57%) was acquired from Yakuri pure chemicals Co., Ltd., Japan. Hydrazine hydrate (N<sub>2</sub>H<sub>4</sub>, 50-60%), nafion and urea were purchased from Sigma-Aldrich Chemical, USA. Methylene blue (C<sub>16</sub>H<sub>18</sub>ClN<sub>3</sub>S, 96%) was purchased from Oriental Chemical Industries Co.,

Ltd., Japan. Sulfuric acid ( $\text{H}_2\text{SO}_4$ , 95%), phosphoric acid ( $\text{H}_3\text{PO}_4$ , 85%), hydrochloric acid ( $\text{HCl}$ , 35-37%), isopropyl alcohol ( $(\text{CH}_3)_2\text{CHOH}$ , 99.5%), ethyl alcohol (94%), acetone (99.5%), and potassium permanganate ( $\text{KMnO}_4$ , 99.3%) were supplied by Duksan Pure Chemicals Co., Ltd., Korea. All chemicals were of the highest purity available and were used as received.

## 2.2 Synthesis of GO

Graphite oxide was prepared from natural graphite powder using a simple room temperature method.<sup>22</sup> Briefly, concentrated sulphuric acid (320 ml) and phosphoric acid (80 ml) was mixed in order with graphite (3 g). With vigorous stirring, 18 g of potassium permanganate was added gradually over a 12 h period. The mixing process was then continued for more 5 days to allow the oxidation of graphite. During oxidation, the color of the mixture changed from dark purplish-green to dark brown. The reaction was quenched by adding approximately 30 mL  $\text{H}_2\text{O}_2$  (dropwise), realizing that the color changed to bright yellow. The graphite oxide formed was collected by centrifugation and washed on a centrifuge with 1 M  $\text{HCl}$  (3 times) and deionized water (several times). During washing with deionized water, the graphite oxide underwent exfoliation, which resulted in thickening of the graphene oxide solution, forming a graphene oxide gel. The final product material was dried in a vacuum at 333 K.

## 2.3 Synthesis of $\text{RGO}_{\text{HI-AcOH}}$

Chemically reduced graphene oxide was fabricated using the method reported elsewhere.<sup>23</sup> 0.4 g of the as-synthesized GO was dispersed in 150 ml of acetic acid. This dispersion was sonicated using Powersonic 420 (Hwashin Technology Company, Republic of Korea) until it became clear with no visible particulate matter. HI (8 ml) was then added and the mixture was then stirred for 24 hours at 40°C. The product was isolated by filtration and washed sequentially with saturated sodium bicarbonate (500 ml), distilled water (500 ml) and acetone

(200 ml). The product was then vacuum dried at room temperature.

#### 2.4 Synthesis of RGO/Ni nanoparticle composites

RGO/Ni nanoparticle composites were prepared using a facile one-step hydrothermal method by controlling the mass ratio of RGO and Ni as 1:1 (G1N1), 2:1 (G2N1), 4:1 (G4N1), 10:1 (G10N1), and 1:2 (G1N2) using the as-synthesized GO and NiCl<sub>2</sub>·6H<sub>2</sub>O at compositions of 20:80, 30:61, 50:50, 70:28, 11:89 mg/mg, respectively. The appropriate amount of GO was dispersed in 30 ml of distilled water by sonication for 2 h to make a GO suspension, followed by the addition of an aqueous solution (10 ml) of the corresponding amount of NiCl<sub>2</sub>·6H<sub>2</sub>O. The mixture was then stirred for 4 h to complete the ion exchange, and urea (0.1 g) and N<sub>2</sub>H<sub>4</sub> (1 ml) were then added with constant stirring. The mixture solution was transferred to a hydrothermal reactor at 140 °C for 12 h. After cooling naturally to room temperature, the resulting black solid was filtered off, washed with distilled water (500 ml) and vacuum dried at room temperature. For comparison, RGO was also prepared using the same method without adding Ni salt, whereas urea was not used during its fabrication.

#### 2.5 Material characterizations

The synthesized materials were characterized by X-ray diffraction (XRD), scanning electron microscopy (SEM), atomic force microscopy (AFM), X-ray photoelectron spectroscopy (XPS), and Raman spectroscopy. The XRD patterns were recorded on a powder X-ray diffractometer (D8 advance, Bruker, Germany) with Cu-K $\alpha$  radiation ( $\lambda = 1.5406 \text{ \AA}$ ) operating at 40 kV and 30 mA. SEM images were obtained using a field-emission scanning electron microscope (S-4200, Hitachi, Japan). AFM measurements were carried out with a Nanoscope IIIa Multimode AFM apparatus (DI instruments, Veeco, USA) under ambient conditions. XPS data were determined using a Thermo Scientific

K-Alpha XPS system (Thermo Fisher Scientific, UK) that is equipped with a monochromatic Al K $\alpha$  source with a spot size of 400  $\mu\text{m}$  and a pass energy of 30 eV. The peaks were fitted and analyzed using Thermo Scientific™ Avantage software (version 5.932). Raman spectra were collected from a Raman spectroscopy (HORIBA Jobin Yvon LabRAM HR, France). Besides, the specific surface area of as-synthesized samples was determined using the methylene blue (MB) adsorption method. (see Supplementary Information for details).

## 2.6 Electrochemical measurements

All electrochemical measurements were performed on an Autolab PGSTAT128N electrochemical workstation (Metrohm Autolab B.V., The Netherlands) using a three-electrode cell at ambient temperature. The as-synthesized electrode materials, platinum electrode and Ag/AgCl (3 M KCl) electrode were used as the working electrode, counter electrode and reference electrode, respectively. The synthesized samples were mixed with isopropyl alcohol and 15 wt% nafion (through sonication), and then deposited on a rectangular-shaped piece (1 $\times$ 1 cm) of non-wet proof carbon cloth substrate (type B-1A, E-TEK, USA) using a simple drop-drying process at ambient temperature to prepare the working electrode. The total mass of material in each electrode (1.4 - 2.6 mg) was determined by measuring the weight change of the carbon cloth before and after material loading.<sup>24,25</sup> Before deposition, the carbon cloth substrate was cleaned by sequential sonication (15 min each) in acetone, 1 M HCl solution, deionized water, and ethanol; followed by drying. The sample loaded substrate was compressed before any measurements. Each experiment was repeated three times with a new pair of sample working electrode. The three experiments indicate a very good reproducibility of as-prepared sample electrodes. Control experiments also confirmed that the capacitance contribution from the carbon cloth substrate was

negligible.

The electrolyte solution was 50 mM phosphate buffer saline (PBS), pH 7.4, containing 0.13g/L KCl, 3.32 g/L NaH<sub>2</sub>PO<sub>4</sub>·2H<sub>2</sub>O, 10.32g/L Na<sub>2</sub>HPO<sub>4</sub>·12H<sub>2</sub>O, and 0.31g/L NH<sub>4</sub>Cl. Cyclic voltammetry (CV) was conducted between 0.5 and -0.2 V (vs. Ag/AgCl) at different scan rates (10 to 500 mV s<sup>-1</sup>). The specific capacitance (Cs, F g<sup>-1</sup>) derived from the CV experiments was calculated using the following equation:

$$Cs = \frac{\int_{V_1}^{V_2} I(V) dV}{\Delta V \cdot v \cdot m} \quad (1)$$

In this equation, the numerator is used to calculate the area under the CV curve,  $\Delta V$  is the potential window (V),  $v$  is the scan rate (V s<sup>-1</sup>), and  $m$  is the mass of the active material on a carbon cloth substrate that determined by weight differences (g). Electrochemical impedance spectroscopy (EIS) was carried out over the frequency range from 100 kHz to 1 Hz at a bias potential of -0.2 V with an amplitude of 5 mV. The galvanostatic charge/discharge curves were measured over the potential range of 0.5 and -0.2 V (vs. Ag/AgCl) at various current densities (0.2 to 1 A g<sup>-1</sup>). The specific capacitance (Cs, F g<sup>-1</sup>), from the galvanostatic charge/discharge plots, was calculated using the following equation:

$$Cs = \frac{I \cdot \Delta t}{\Delta V \cdot m} \quad (2)$$

where  $I$  is the current (A),  $\Delta t$  is the discharge time (s),  $\Delta V$  is the potential window (V), and  $m$  is the mass of active material on a carbon cloth substrate that determined by weight differences (g).

### 3. Results and discussion

#### 3.1 Material characterizations

Fig. 1 shows XRD patterns of the as-prepared samples. The pure GO showed a typical

diffraction peak (002) at  $10.6^\circ 2\theta$ . The broad and weak peaks at approximately  $24 \sim 26^\circ 2\theta$  were assigned to the (002) diffraction of the RGO. The shift of the XRD pattern of GO ( $10.6^\circ$ ) to RGO ( $24 \sim 26^\circ$ ) indicated the successful reduction of GO by HI-AcOH and hydrazine hydrate. The characteristic peaks at approximately  $44^\circ$ ,  $51^\circ$ , and  $76^\circ 2\theta$  correspond to the (111), (200) and (220) crystal planes of spherical-like Ni nanoparticles. These characteristic peaks from crystal Ni showed that the nickel ions had possibly been reduced to Ni nanoparticles after the reducing process. The data are consistent with that reported in the literatures.<sup>23, 26, 27</sup> In the RGO/Ni nanoparticle composites (G1N1, G2N1, G4N1, G10N1), the characteristic peak of RGO emerged gradually with increasing RGO to Ni nanoparticle mass ratio. Accordingly, the characteristic peak of Ni decreased in intensity (G1N1: 4553 a.u., G2N1: 2971 a.u., G4N1: 2376 a.u., and G10N1: 585 a.u.). With G1N2 composite, a higher Ni to RGO mass ratio represents a higher intensity (6062 a.u.) of Ni characteristic peaks as compared to others.

SEM was used to investigate the surface morphologies of as-prepared GO, RGOs and RGO/Ni nanoparticle composite samples prior to deposition (Fig. 2). GO appears to have been successfully exfoliated to some extent (Fig. 2a), and was further exfoliated to RGOs (Fig. 2b and c). GO was found to have a flaky texture that reflected its layered structure consisting of several stacking sheets of GO. The RGO<sub>HI-AcOH</sub> has crumpling features with clear layers, which could be responsible for creating the ultimate high surface area and surface nanostructure in RGO<sub>HI-AcOH</sub>. The RGO<sub>hydrazine</sub> showed a rippled and paper sheet-like structure that was assembled on one another. Figs. 2d to 2h also reveals a considerable growth of spherical-like Ni nanoparticle on or between the RGO layers, depending on the mass ratio, which might hinder aggregation. These nanoparticles were relatively uniform in size and stacked randomly in the RGO layers. The proportion of Ni nanoparticles obtained

decreased with increasing ratio of RGO (as G1N1, G2N1, G4N1, G10N1) in the composites. Similarly, the proportion of RGO decreased when the ratio of Ni nanoparticles in the composite sample was increased (as G1N2).

Atomic force microscopy (AFM) was employed to evaluate the thickness and layer numbers of as prepared GO and RGOs (Fig. 3). Section analysis revealed that the thickness of GO is about 1.13 nm (Fig. 3a). From the AFM images (Fig. 3b and c), the thickness of RGO<sub>hydrazine</sub> and RGO<sub>HI-AcOH</sub> are also estimated to be about 2.46 nm and 7.36 nm, respectively. Here, it should be noted that a pure single layer graphene has a thickness of 0.34 nm which is corresponding to the interlayer spacing of graphite whereas a GO is  $\sim 1$  nm thick due to the presence of functional groups, structural defects and adsorbed water molecules.<sup>28</sup> From this, it was reasonable to assume that the GO contains about 1 layer. Accordingly, the RGO<sub>hydrazine</sub> and RGO<sub>HI-AcOH</sub> are consisted, respectively, of about 7 and 22 layers. The multilayer graphene could be a viable electrode material, where the conductivity of few layers is insufficient.<sup>29</sup>

XPS was performed to validate the successful conjugation of GO, RGOs and RGO/Ni nanoparticale composite (as G1N1) (Fig. 4). According to the XPS survey spectrum (0-1350 eV), all the as-prepared samples shows carbon, oxygen and nickel as the main species (Fig. 4a). C1s XPS of pure GO revealed a high degree of oxidation with five different carbon environments of C=C (284 eV), C-C (284.6), C-O (285.5 eV), C=O (287 eV), O-C=O (288.4 eV) groups (Fig. 4b-i).<sup>30</sup> The C1s XP spectrum of the RGO samples (Fig. 4b-ii and -iii) and G1N1 composite (Fig. 4b-iv) showed the characteristic peaks of C=C at  $284 \pm 0.1$  eV, C-C at  $284.6 \pm 0.04$  eV, C-O at  $285.3 \pm 0.2$  eV, C=O at  $286.2 \pm 0.2$  eV, and O-C=O at  $288.1 \pm 0.1$  eV. In addition, a  $\pi$ - $\pi^*$  shake up satellite peak was observed at around 293 eV (for GO) and 291 eV (for RGOs and G1N1 composite). All oxygenated functional groups containing the

characteristic peaks of C-O, C=O and O-C=O were decreased significantly after the HI-AcOH and hydrazine treatment. The C and O elements with an atomic ratio of 1.2 for GO were obtained from XPS analysis, whereas the C/O atomic ratio of RGO<sub>HI-AcOH</sub> and RGO<sub>hydrazine</sub> were found to be 5.17, and 3.94, respectively; suggesting the successful reduction of RGOs. A greater C/O ratio (5.17 (RGO<sub>HI-AcOH</sub>) vs. 3.94 (RGO<sub>hydrazine</sub>)) can lead to a higher current conductivity of graphene materials that indicates the efficiency of a particular reduction method.<sup>31</sup> The Ni2p spectrum (Fig. 4c) suggests that Ni has a zero-valence at binding energies 855.8 eV and 873.6 eV. The two weak peaks at binding energies of 857.6 and 876.4 were assigned to the divalent form of nickel (Ni<sup>2+</sup>). The satellite peaks due to the shake-up processes were centered at 861.2 eV, 863.6 eV and 880 eV. These assignments are in agreement with previous studies.<sup>27, 32</sup> The small fraction of Ni<sup>2+</sup> in the G1N1 composite may be understood either as the result of surface oxidation of the sample because they are exposed to the atmosphere while being transferred from the deposition chamber to the XPS system, or it can be due to adsorption by OH (or H<sub>2</sub>O) species during its fabrication. Besides all these, the residual plots show a good fit to the data in the spectrums obtained by XPS (Fig. S2).

Raman spectroscopy was performed to elucidate the graphitic structure of GO, RGOs and the interactions among RGO, and Ni nanoparticles (as G1N1) (Fig. 5). The data obtained from these experiments also summarizes in Table 1. All Raman spectra display the typical bands with relevant position values expected for carbonaceous materials namely the D band ( $\sim 1350\text{ cm}^{-1}$ ), the G band ( $\sim 1592\text{ cm}^{-1}$ ), and the 2D band ( $\sim 2707\text{ cm}^{-1}$ ).<sup>33</sup> The D band related to the presence of disorder in the sp<sup>2</sup> carbon network, the G band associated with the sp<sup>2</sup> carbon atom vibrations along the structure axis, and the 2D band corresponding to a second order dispersive Raman mode. Compared with GO (Fig. 5a), the blue shift of D and G

bands and the red shift of 2D band in RGOs (Fig. 5b and c) and G1N1 composite (Fig. 5d) indicated exfoliation of the RGO sheets. However, in G1N1 composite, the presence of Ni nanoparticles in the graphene structure gives rise to a red shift in the 2D band (compared to RGOs) as a result of the interaction between the reduced graphene oxide and Ni nanoparticles. On the other hand, the increased  $I_D/I_G$  ( $I_D$  = intensity of D band,  $I_G$  = intensity of G band) ratio of RGO after the chemical reduction is commonly stated by the previous literature.<sup>34</sup> In the present study, the  $I_D/I_G$  ratio of RGOs and G1N1 composite exhibited an increase compared to GO. In the case of  $\text{RGO}_{\text{HI-AcOH}}$ , the  $I_D/I_G$  ratio was found to be higher than others, showing better graphitization.

The MB adsorption method is widely accepted in the literature as a more reliable method for determining the surface area of graphene-based materials, compared with the BET nitrogen adsorption.<sup>35</sup> In that order, by MB adsorption method, the specific surface area of RGOs and RGO/Ni nanoparticle composite (as G1N1) was derived at complete cation replacement phase (Fig. S1). At this point, from the amount of adsorbed MB, specific surface area was calculated (using equation S1). The results illustrated that  $\text{RGO}_{\text{HI-AcOH}}$  has a specific surface area of  $343 \text{ m}^2 \text{ g}^{-1}$ , which is higher than that of  $\text{RGO}_{\text{hydrazine}}$  ( $208 \text{ m}^2 \text{ g}^{-1}$ ) and G1N1 composite ( $245 \text{ m}^2 \text{ g}^{-1}$ ) samples.

### 3.2 Electrochemical properties

Fig. 6a shows the cyclic voltammetry (CV) curves of the different electrodes at a scan rate of  $10 \text{ mV s}^{-1}$ . Obviously,  $\text{RGO}_{\text{HI-AcOH}}$  has a higher specific capacitance ( $39.72 \text{ F g}^{-1}$ ) at the same scan rate (using equation 1) than those of  $\text{RGO}_{\text{hydrazine}}$  ( $24.69 \text{ F g}^{-1}$ ), G1N1 ( $29.56 \text{ F g}^{-1}$ ), G2N1 ( $27.43 \text{ F g}^{-1}$ ), G4N1 ( $25.04 \text{ F g}^{-1}$ ), G10N1 ( $24.78 \text{ F g}^{-1}$ ), and G1N2 ( $8.40 \text{ F g}^{-1}$ ), which highlights the excellent electrochemical performance of its electrode material. This could be attributed to the high degree of deoxygenation and high graphitization without

nitrogen incorporation by  $\text{RGO}_{\text{HI-AcOH}}$ .<sup>23</sup> Among the as-prepared RGO/Ni nanoparticle composite electrodes, G1N1 had the highest specific capacitance at the same scan rate. From a structural point of view, nanoparticles are primarily acting as spacers to prevent the restacking of graphene sheets. The good electrochemical performance of G1N1 can be attributed to the appropriate mass ratio of the RGO/Ni nanoparticles in the composite leading to less aggregation of graphene and a good dispersion of Ni nanoparticles on the graphene surface, which causes a higher active surface area for charge storage. With increasing mass ratio of RGO in the composite samples (e.g., G2N1, G4N1 and G10N1), the specific capacitance decreased to the level of the produced-hydrazine RGO. This instability was attributed mainly to the presence of a high proportion of RGO causing more aggregation. G1N2 showed the smallest specific capacitance compared to the other electrodes at the same scan rate. The significant decrease in the specific capacitance of the G1N2 composite electrode suggests a weak synergistic effect of metal nanoparticles at high loading deposition where the surface of RGO can assume to have no longer accessible to the electrolyte. As a result, the metal nanoparticles did not appear to be electrochemically active within the explored potential window apart from acting as a spacer. In addition, the CV curves at various scan rates were studied to obtain more detailed information on the capacitance performance of the as-prepared electrodes (Fig. 6b). The specific capacitance decreased gradually with increasing scan rate. Such a decrease was attributed to the insufficient time available for ion diffusion and adsorption inside the smallest pores within a large particle at high scan rates.<sup>9</sup> On the other hand, the  $\text{RGO}_{\text{HI-AcOH}}$  electrode still retains good capacitive behavior even at high scan rates.

Fig. 7 presents the EIS Nyquist plots of the different electrodes. All the plots were made up of a single semicircle in the high frequency region followed by a straight line in the low

frequency due to a diffusion process (Warburg diffusion). The intersection point of the semicircle on the real axis at high frequency represents the equivalent series resistance ( $R_s$ ) of the electrodes, whereas the diameter of the semicircle corresponds to the charge-transfer resistance ( $R_{CT}$ ) of the electrodes and electrolyte interfaces.<sup>36</sup> From this, it is apparent that RGO<sub>HI-AcOH</sub> electrode has the lowest series resistance ( $R_s$ ), smallest charge-transfer resistance ( $R_{CT}$ ), and the utmost ideal straight line, indicating a lower intrinsic resistance, faster electrolyte diffusion, and better electrical conductivity and capacitive behavior than other electrodes. The faster electrolyte diffusion in RGO<sub>HI-AcOH</sub> could be attributed to its higher surface area that is in contact with the electrolyte (as shown by SEM images and MB test results). In particular, the RGO<sub>HI-AcOH</sub> has a multi-layer structure and a higher graphitization degree than hydrazine-produced RGO based materials according to the AFM, XPS and Raman analysis, and thus the higher conductivity is obtained.<sup>29, 31</sup> Ni nanoparticles act merely as spacers to increase the interlayer spacing between RGO sheets. Regardless of the impedance performance of RGO<sub>HI-AcOH</sub>, the G1N1 composite electrode showed a lower intrinsic resistance and a predominant straight line compared to others. The straight line for the G1N1 composite corresponds to an appropriate mass ratio of the RGO/Ni nanoparticles, which allows easier diffusion of the electrolyte across the interface between nanoparticles and graphene sheets. By further increasing the mass ratio of the RGO/Ni nanoparticles (as G2N1, G4N1, G10N1), the charge-transfer resistance ( $R_{CT}$ ) increased while Warburg diffusion process is limited due to aggregation of graphene layers. The G1N2 composite exhibited the largest charge-transfer resistance ( $R_{CT}$ ). Accordingly, longer electrolyte diffusion pathway can be assigned for G1N2 composite as a result of the high mass ratio of nanoparticles that limiting the active sites accessible by an electrolyte.

Based on the above findings, the RGO<sub>HI-AcOH</sub> and G1N1 composite electrodes were chosen as

a reasonable preference for subsequent studies. Accordingly, galvanostatic charge/discharge analysis was conducted to gain fundamental insight into behaviors of these electrodes for supercapacitor applications. Fig. 8a shows galvanostatic charge-discharge measurements of the RGO<sub>HI-AcOH</sub> and G1N1 composite electrodes at a constant current density of 0.2 A g<sup>-1</sup>. The shapes of the charge/discharge curves are closely triangular in shape, suggesting good reversibility during the charge/discharge processes. Apparently, the nonlinear behavior of the galvanostatic charge-discharge could be attributed to available contact surface area that promotes ion adsorption and diffusion. The much longer charge/discharge time of the RGO<sub>HI-AcOH</sub> electrode highlighted its preferable electrochemical performance to that of the G1N1 composite electrode. Similarly, the RGO<sub>HI-AcOH</sub> electrode (69.43 F g<sup>-1</sup> at 0.2 A g<sup>-1</sup>) exhibited a higher specific capacitance (using equation 2) than the G1N1 composite electrode (26.63 F g<sup>-1</sup> at 0.2 A g<sup>-1</sup>). The high supercapacitance potential of the RGO<sub>HI-AcOH</sub> is possibly due to a high degree of graphitization without nitrogen incorporation. This finding is in agreement with the CV and EIS results. As expected, the specific capacitance decreased with increasing current density in both cases (Fig. 8b). Despite this, RGO<sub>HI-AcOH</sub> still showed a high specific capacitance compared to the G1N1 composite electrode even when the current density was increased up to 1 A g<sup>-1</sup>. These are consistent with that obtained from the CV result, as explained in Fig. 6b. The lower capacitance at high current rates can be due to the inadequate time for electrolyte diffusion into the inner pores. In addition, a cyclic stability test was performed on the RGO<sub>HI-AcOH</sub> electrode by charge-discharge experiments at a constant current density of 0.2 A g<sup>-1</sup> for 1000 cycles (Fig. 9). There was a small decrease (6.35%) in the specific capacitance during the first 200 cycles and then remained almost constant over the full cycle (93.65% retention). This indicates the excellent stability (life-time) of the RGO<sub>HI-AcOH</sub> electrode, which can be used sustainably as an ideal energy storage device for

supercapacitor applications.

It should be recognized that a direct comparison of the present results with other reported data is quite difficult because it is not easy to find similar studies due to the different types of substrates, active materials, synthesis methods, and electrode preparation methods used. These factors can strongly affect the performance of supercapacitors.<sup>37</sup> However, such interest comparison based-single RGO electrode materials donating specific capacitance of charge-discharge studies is presented in Table S1. It seems that the performance of RGO<sub>HI-AcOH</sub> electrode is relative low compared with those previously reported in the literatures. But, it highlights the green method for the synthesis of RGO, which is worth to be encouraged. Future research needs in using various substrate and deposition method to meet the high performance supercapacitor electrode. Here, there is evidence suggesting that a higher specific capacitance could be obtained using other matrix substrates, whereas there are associated drawbacks with other substrates as explained elsewhere.

#### 4. Conclusions

The paper reported the potential use of high conductive graphene material (RGO<sub>HI-AcOH</sub>) instead of graphene nanoparticle composites (RGO/Ni) in supercapacitors. RGO<sub>HI-AcOH</sub> and produced-hydrazine RGO and RGO/Ni nanoparticles composites were synthesized (indicated by XRD, SEM, AFM, XPS, and raman spectroscopy) as electrode materials (coated on a carbon cloth substrate) for electrochemical capacitors. RGO<sub>HI-AcOH</sub> possessed a higher MB specific surface area (~1.5-2 times) than RGO<sub>hydrazine</sub> and RGO/Ni nanoparticales composite (as G1N1). Compared to the other electrodes, the RGO<sub>HI-AcOH</sub> electrode exhibited the highest performance with a specific capacitance of 40 F g<sup>-1</sup> at 10 mV s<sup>-1</sup>, and 70 F g<sup>-1</sup> at 0.2 A g<sup>-1</sup>. Moreover, it had good specific capacitance retention of ~94% up to 1000 continuous charge/discharge cycles. The high supercapacitance performance of the RGO<sub>HI-AcOH</sub> was

attributed mainly to the high surface area and degree of graphitization without nitrogen deposition caused by hydrazine hydrate. Interestingly, the RGO to Ni nanoparticles mass ratio (or vice versa) in the composite samples has a great influence on their electrochemical performance. The same phenomena could possibly be obtained by using other nanoparticles. Among the nanoparticle composites prepared, RGO/Ni at the correspond mass ratio of 1:1 (G1N1) showed better electrochemical performance than those of the hydrazine RGO and other graphene nanoparticle composites, possessing an optimal capacitance of  $30 \text{ F g}^{-1}$  at  $10 \text{ mV s}^{-1}$ , and  $27 \text{ F g}^{-1}$  at  $0.2 \text{ A g}^{-1}$ . The general pathway of these studies shows that RGO<sub>HI-AcOH</sub> material, particularly when combined with a flexible carbon cloth substrate, could be a promising candidate for practical applications in energy storage devices. However, to reach fruition, further research will be needed.

### Acknowledgment

This study was supported by Basic Science Research Program through the National Research Foundation of Korea (NRF) funded by the Ministry of Science, ICT and Future Planning (NRF-2014R1A2A2A04002446).

### References

- 1 S. Maiti, A.K. Das, S.K. Karan and B.B. Khatua, *J. Appl. Polym. Sci.*, 2015, **132**, 42118-42123.
- 2 J. Xiao, Y. Xu and S. Yang, High-performance supercapacitors based on novel graphene composites, in: A.R. bin Mohd Yusoff (Ed.), *Graphene-based Energy Devices*, Wiley-VCH, Germany, 2015, pp. 145-171.
- 3 A. Singh and A. Chandra, *AIP Conf. Proc.*, 2013, **1538**, 253- 256.
- 4 M. Skoda, I. Dudek, A. Jarosz and D. Szukiewicz, *J. Nanomater.*, 2014, **2014**, 1-11.

- 5 S. Gurunathan, J.W. Han, E. Kim, D.-N. Kwon, J.-K. Park and J.-H. Kim, *J. Nanobiotechnol.*, 2014, **12**, 41-57.
- 6 G. Shi, Gelation of graphene oxide, in: V. Mittal (Ed.), *Polymer-Graphene Nanocomposites*, RCS, UK, 2012, pp. 52-65.
- 7 S. Bai, X. Shen, G. Zhu, M. Li, H. Xi and K. Chen, *ACS Appl. Mat. Interfaces*, 2012, **4**, 2378-2386.
- 8 J. Chang, H. Xu, J. Sun and L. Gao, *J. Mater. Chem.*, 2012, **22**, 11146-11150.
- 9 Z. Li, Z. Zhou, G. Yun, K. Shi, X. Lv and B. Yang, *Nanoscale Res. Lett.*, 2013, **8**, 473-482.
- 10 W. Lu, X. Qin, A.M. Asiri, A.O. Al-Youbi and X. Sun, *Analyst*, 2013, **138**, 429-433.
- 11 A. Ramadoss, G.-S. Kim and S.J. Kim, *CrystEngComm*, 2013, **15**, 10222-10229.
- 12 H. Yu, J. He, L. Sun, S. Tanaka and B. Fugetsu, *Carbon*, 2013, **51**, 94-101.
- 13 D. Sun, X. Yan, J. Lang and Q. Xue, *J. Power Sources*, 2013, **222**, 52-58.
- 14 H. Wang, D. Zhang, T. Yan, X. Wen, J. Zhang, L. Shi and Q. Zhong, *J. Mater. Chem. A*, 2013, **1**, 11778-11789.
- 15 H. Wang, L. Shi, T. Yan, J. Zhang, Q. Zhong and D. Zhang, *J. Mater. Chem. A*, 2014, **2**, 4739-4750.
- 16 J. Bae, M.K. Song, Y.J. Park, J.M. Kim, M. Liu and Z.L. Wang, *Angew. Chem. Int. Ed.*, 2011, **50**, 1683-1687.
- 17 D. Chao, X. Xia, C. Zhu, J. Wang, J. Liu, J. Lin, Z. Shen and H.J. Fan, *Nanoscale*, 2014, **6**, 5691-5697.
- 18 T.T. Vu, Nanostructured Metal Oxides Supported on Stainless Steel Wire Meshes: Versatile Monolithic Catalysts for Environmental and Energy Applications, PhD thesis, Universidad De Oviedo, Spain, 2014.

- 19 Y.-K. Hsu, Y.-C. Chen, Y.-G. Lin, L.-C. Chen and K.-H. Chen, *J. Mater. Chem.*, 2012, **22**, 3383-3387.
- 20 R. Zhang, J. Liu, H. Guo and X. Tong, *Mater. Lett.*, 2014, **136**, 198-201.
- 21 Y. Zou and S. Wang, *Scientific Reports*, 2015, **5**, 11792-11799.
- 22 N.M. Huang, H.N. Lim, C.H. Chia, M.A. Yarmo and M.R. Muhamad, *Int. J. Nanomedicine*, 2011, **6**, 3443-3448.
- 23 I.K. Moon, J. Lee, R.S. Ruoff and H. Lee, *Nat. Commun.*, 2010, **1**, 73-79.
- 24 A.N. Naveen and S. Selladurai, *Electrochim. Acta*, 2014, **125**, 404-414.
- 25 S.I.U. Shah, A.L. Hector and J.R. Owen, *J. Power Sources*, 2014, **266**, 456-463.
- 26 H.-M. Ju, S.-H. Choi and S.H. Huh, *J. Korean Phys. Soc.*, 2010, **57**, 1649-1652.
- 27 B. Li, H. Cao, J. Yin, Y.A. Wu and J.H. Warner, *J. Mater. Chem.*, 2012, **22**, 1876-1883.
- 28 G. Eda, G. Fanchini and M. Chhowalla, *Nat. Nanotechnol.*, 2008, **3**, 270-274.
- 29 M.A. Kuroda, J. Tersoff, D.M. Newns and G.J. Martyna, *Nano Lett.*, 2011, **11**, 3629-3633.
- 30 H.-W. Tien, Y.-L. Huang, S.-Y. Yang, S.-T. Hsiao, W.-H. Liao, H.-M. Li, Y.-S. Wang, J.-Y. Wang and C.-C. M. Ma, *J. Mater. Chem.*, 2012, **22**, 2545-2552.
- 31 C.K. Chua and M. Pumera, *Chem. Soc. Rev.*, 2014, **43**, 291-312.
- 32 T.-Y. Yung, L.-Y. Huang, T.-Y. Chan, K.-S. Wang, T.-Y. Liu, P.-T. Chen, C.-Y. Chao and L.-K. Liu, *Nanoscale Res. Lett.*, 2014, **9**, 444-450.
- 33 E. Nossol, A.B.S. Nossol, S.-X. Guo, J. Zhang, X.-Y. Fang, A.J.G. Zarbin and A.M. Bond, *J. Mater. Chem. C*, 2014, **2**, 870-878.
- 34 P. Cui, J. Lee, E. Hwang and H. Lee, *Chem. Commun.*, 2011, **47**, 12370-12372.
- 35 S.H. Aboutalebi, R. Jalili, D. Esrafilzadeh, M. Salari, Z. Gholamvand, S.A. Yamini, K. Konstantinov, R.L. Shepherd, J. Chen, S.E. Moulton, P.C. Innis, A.I. Minett, J.M. Razal and G.G. Wallace, *ACS Nano*, 2014, **8**, 2456-2466.

36 X. Chen, X. Chen, F. Zhang, Z. Yang and S. Huang, *J. Power Sources*, 2013, **243**, 555-561.

37 D. Yang, Application of nanocomposites for supercapacitors: characteristics and properties, in: F. Ebrahimi (Ed.), *Nanocomposites - New Trends and Developments*, InTech, Croatia, 2012, pp. 299-328.

### Figure Captions

**Fig. 1** XRD patterns of (a) GO, (b) RGO<sub>HI-AcOH</sub>, (c) RGO<sub>hydrazine</sub>, and composite samples with different mass ratio of RGO/Ni nanoparticles as (d) G1N1, (e) G2N1, (f) G4N1, (g) G10N1, and (h) G1N2.

**Fig. 2** SEM images of (a) GO, (b) RGO<sub>HI-AcOH</sub>, (c) RGO<sub>hydrazine</sub>, and composite samples with different mass ratios of RGO/Ni nanoparticles as (d) G1N1, (e) G2N1, (f) G4N1, (g) G10N1, and (h) G1N2.

**Fig. 3** AFM images of (a) GO, (b) RGO<sub>hydrazine</sub>, and (c) RGO<sub>HI-AcOH</sub>.

**Fig. 4** XPS of (a) survey scan, (b) C1s, and (c) Ni2p of the (i) GO, (ii) RGO<sub>HI-AcOH</sub>, (iii) RGO<sub>hydrazine</sub>, and (iv) G1N1 composite samples.

**Fig. 5** Raman spectra of (a) GO, (b) RGO<sub>HI-AcOH</sub>, (c) RGO<sub>hydrazine</sub>, and (d) G1N1 composite.

**Fig. 6** (a) CV curves at a scan rate of  $10 \text{ mV s}^{-1}$ , and (b) specific capacitances calculated from CV at different scan rates for all prepared electrodes.

**Fig. 7** Nyquist impedance plots for all prepared electrodes.

**Fig. 8** (a) galvanostatic charge-discharge curves at a current density of  $0.2 \text{ A g}^{-1}$ , and (b) the specific capacitance calculated from the discharge curves at different current densities for RGO<sub>HI-AcOH</sub> and G1N1 composite electrodes.

**Fig. 9** Variation of the specific capacitance of the RGO<sub>HI-AcOH</sub> electrode as a function of the cycle number at a current density of  $0.2 \text{ A g}^{-1}$ .

Fig. 1

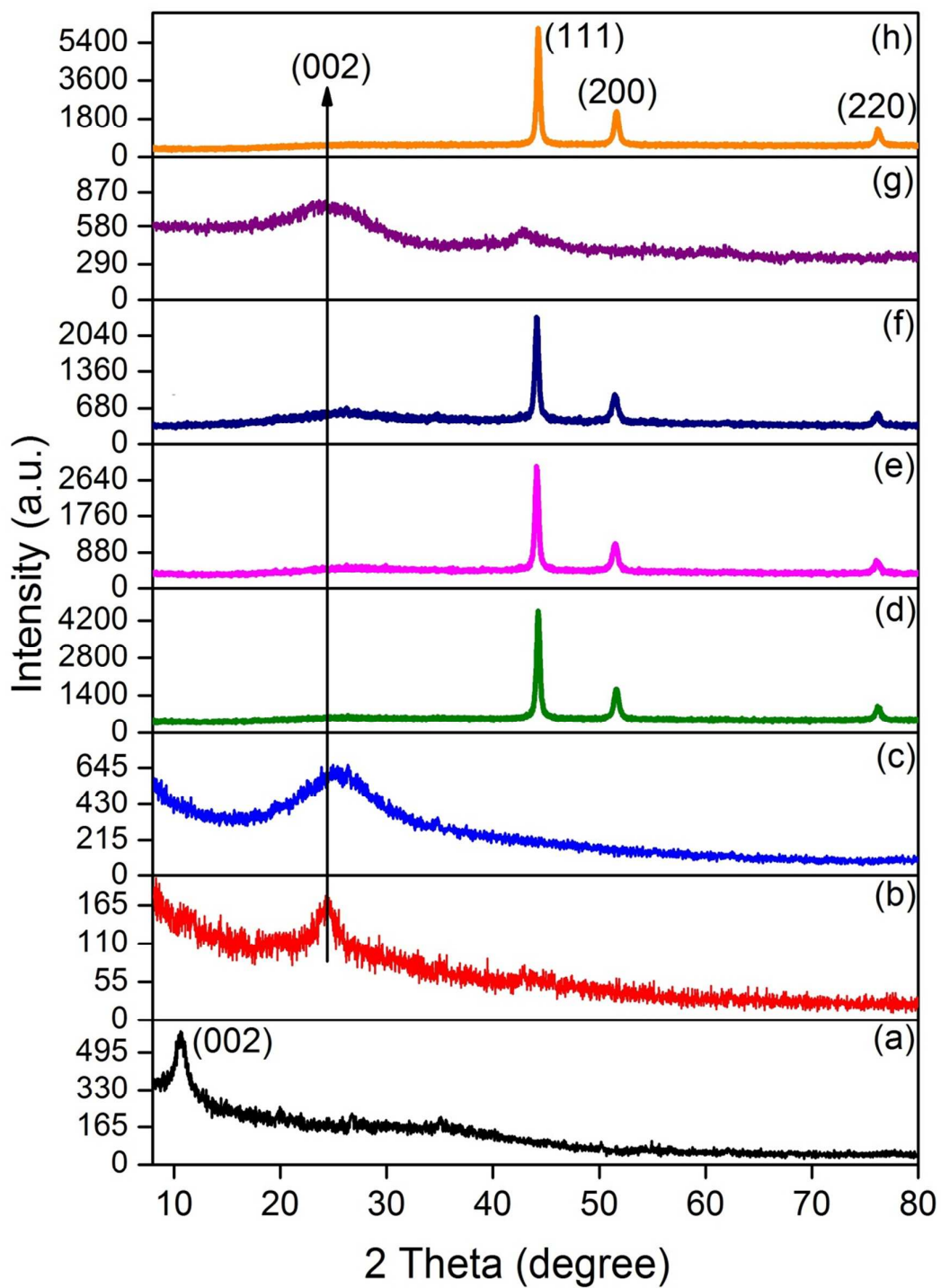


Fig. 2

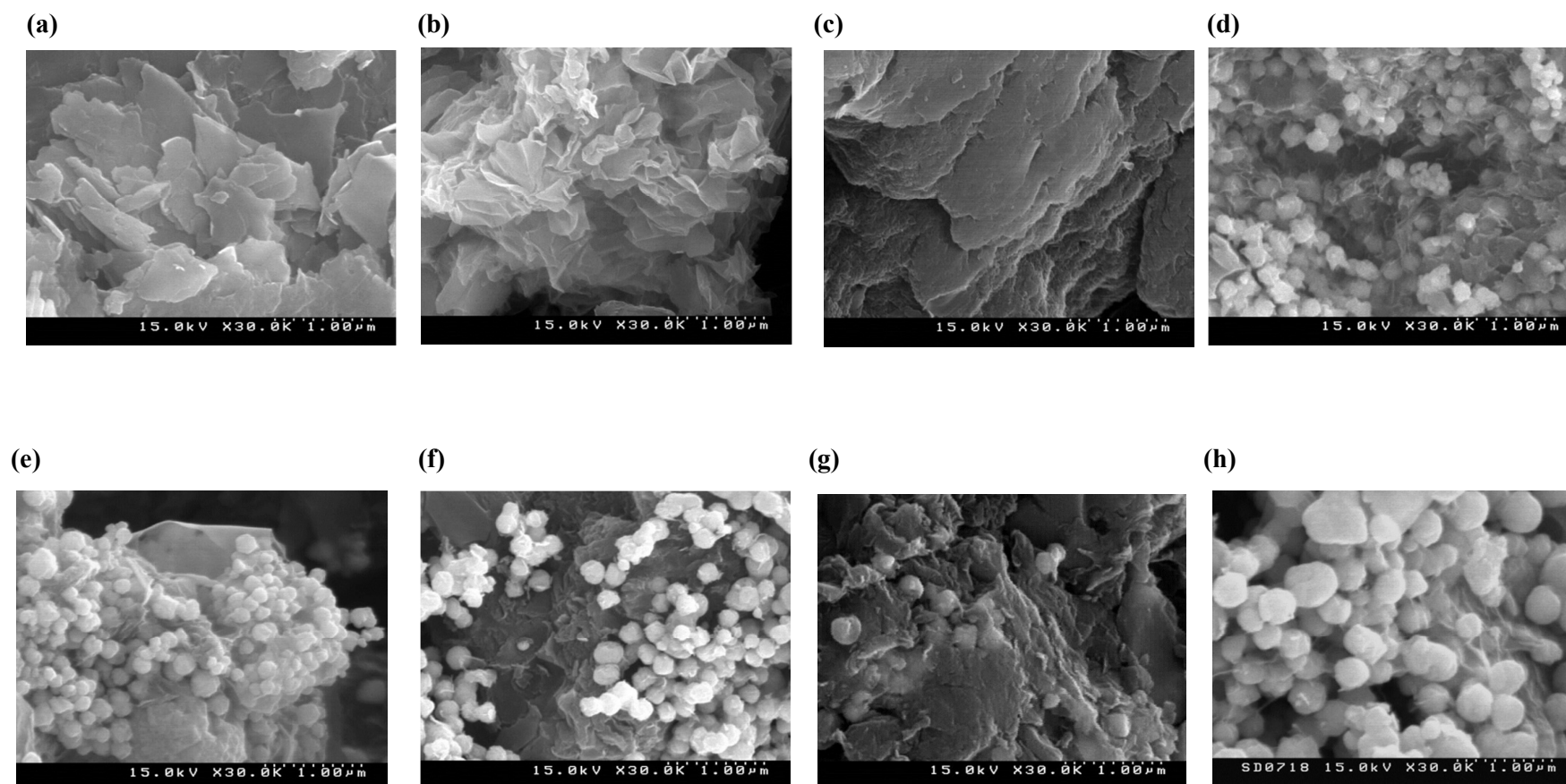


Fig. 3

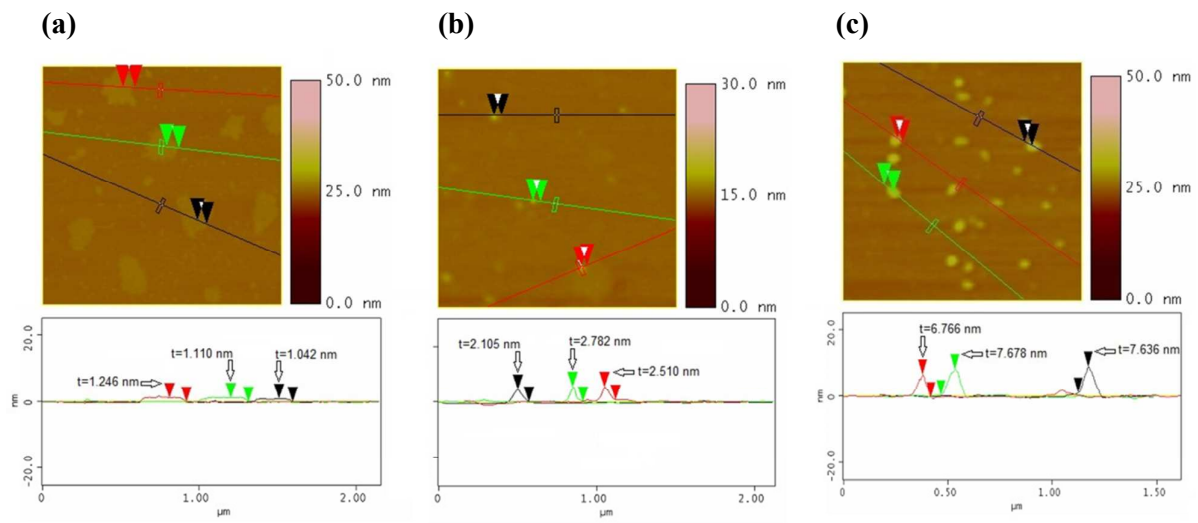


Fig. 4

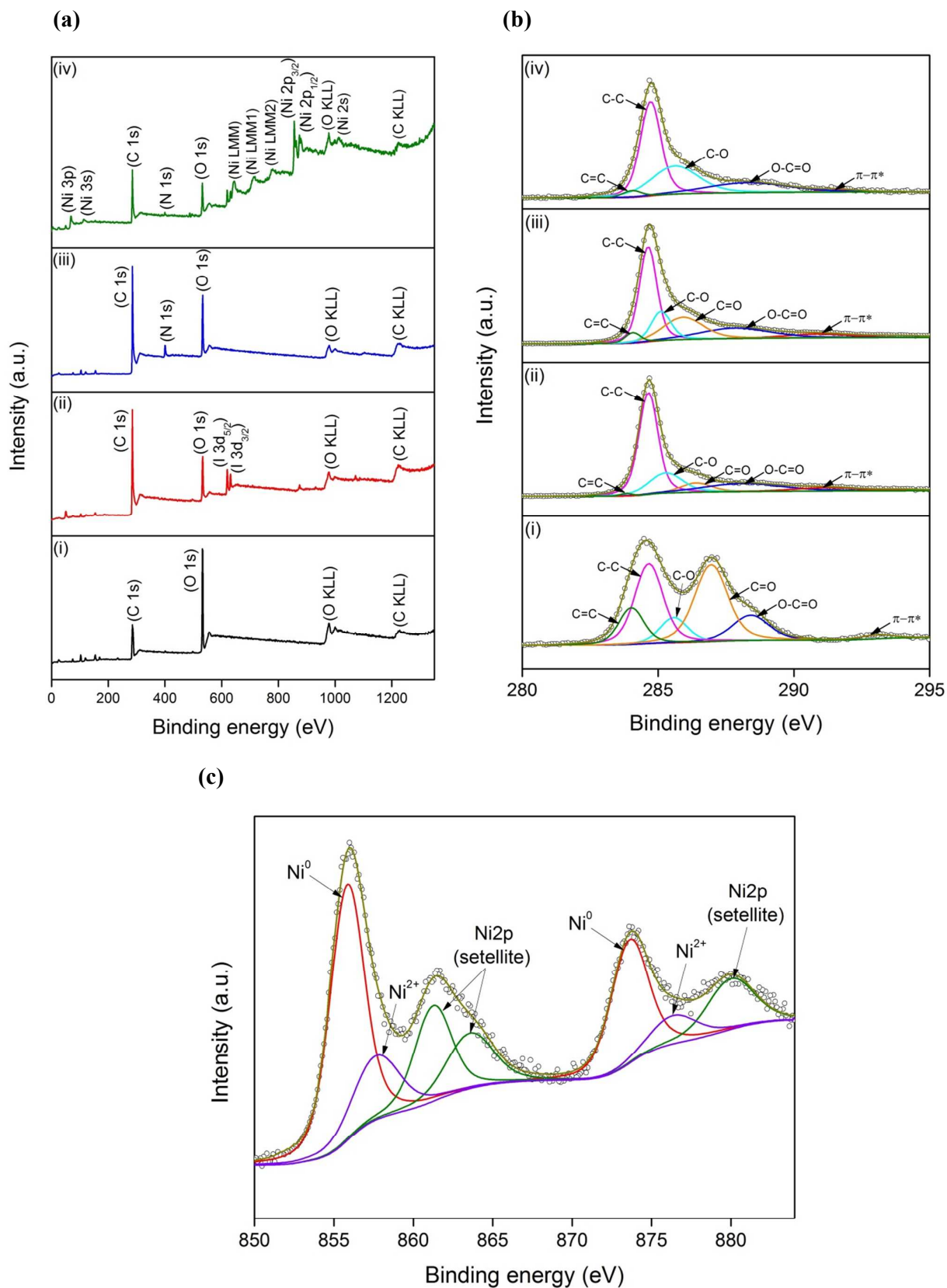


Fig. 5

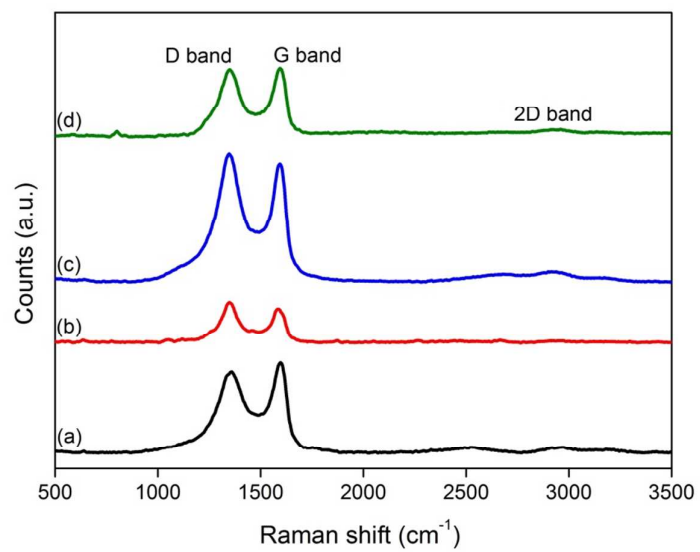


Fig. 6

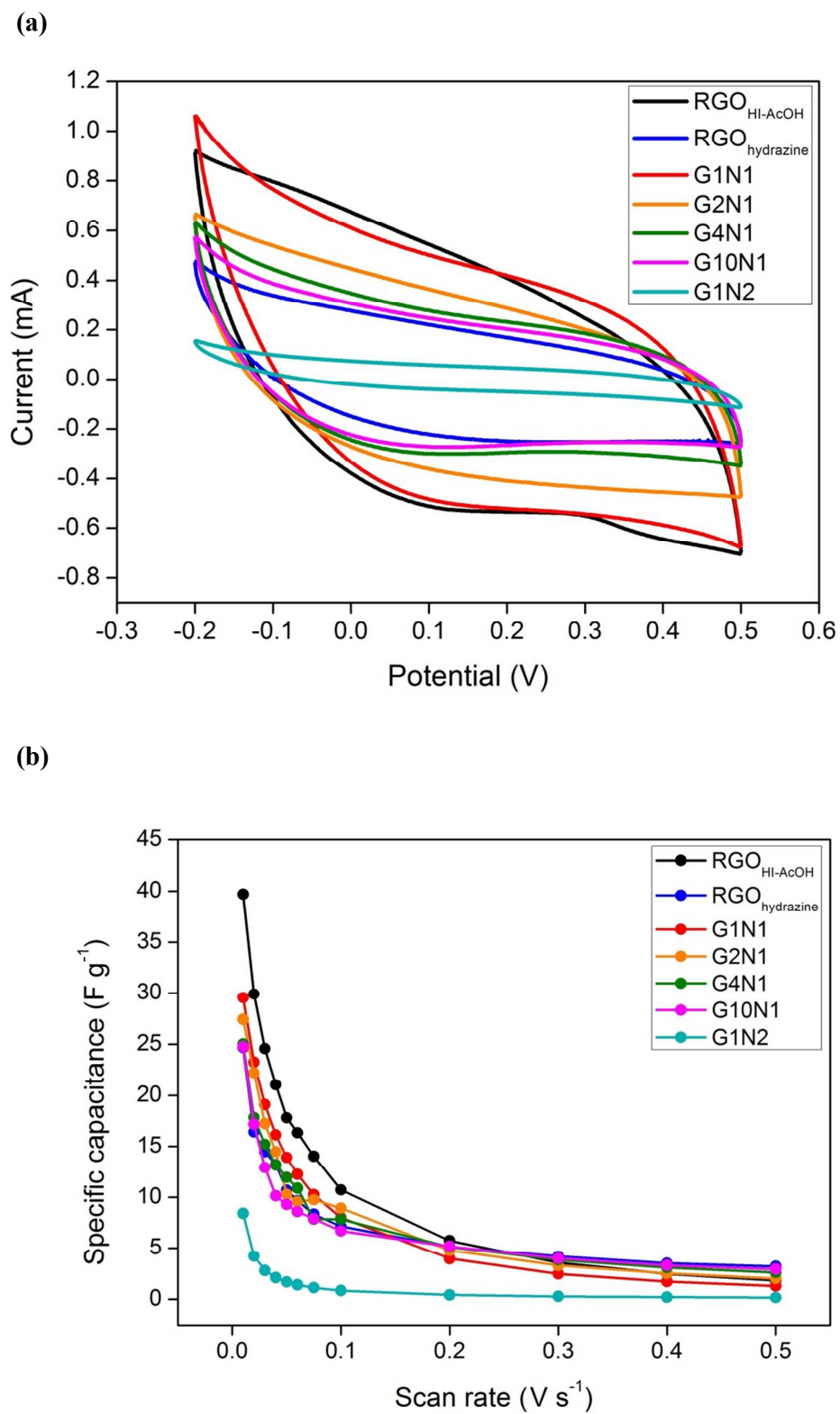


Fig. 7

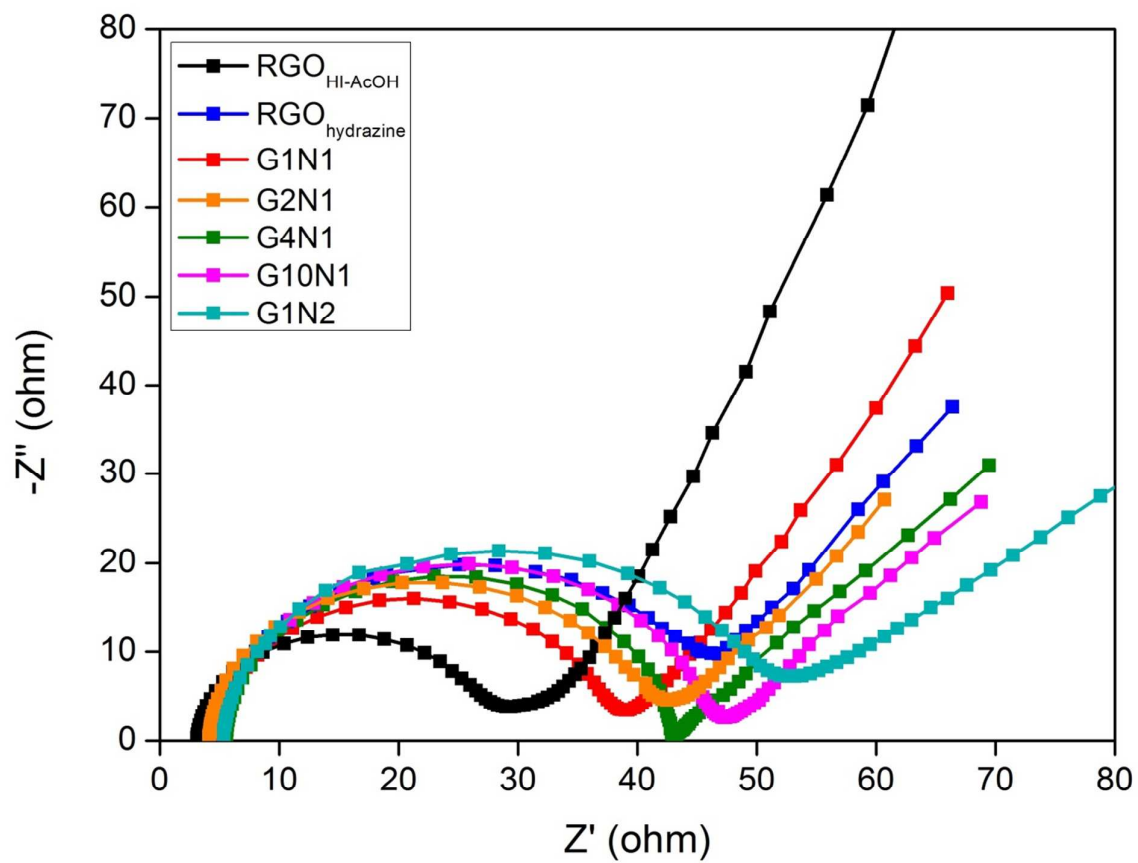


Fig. 8

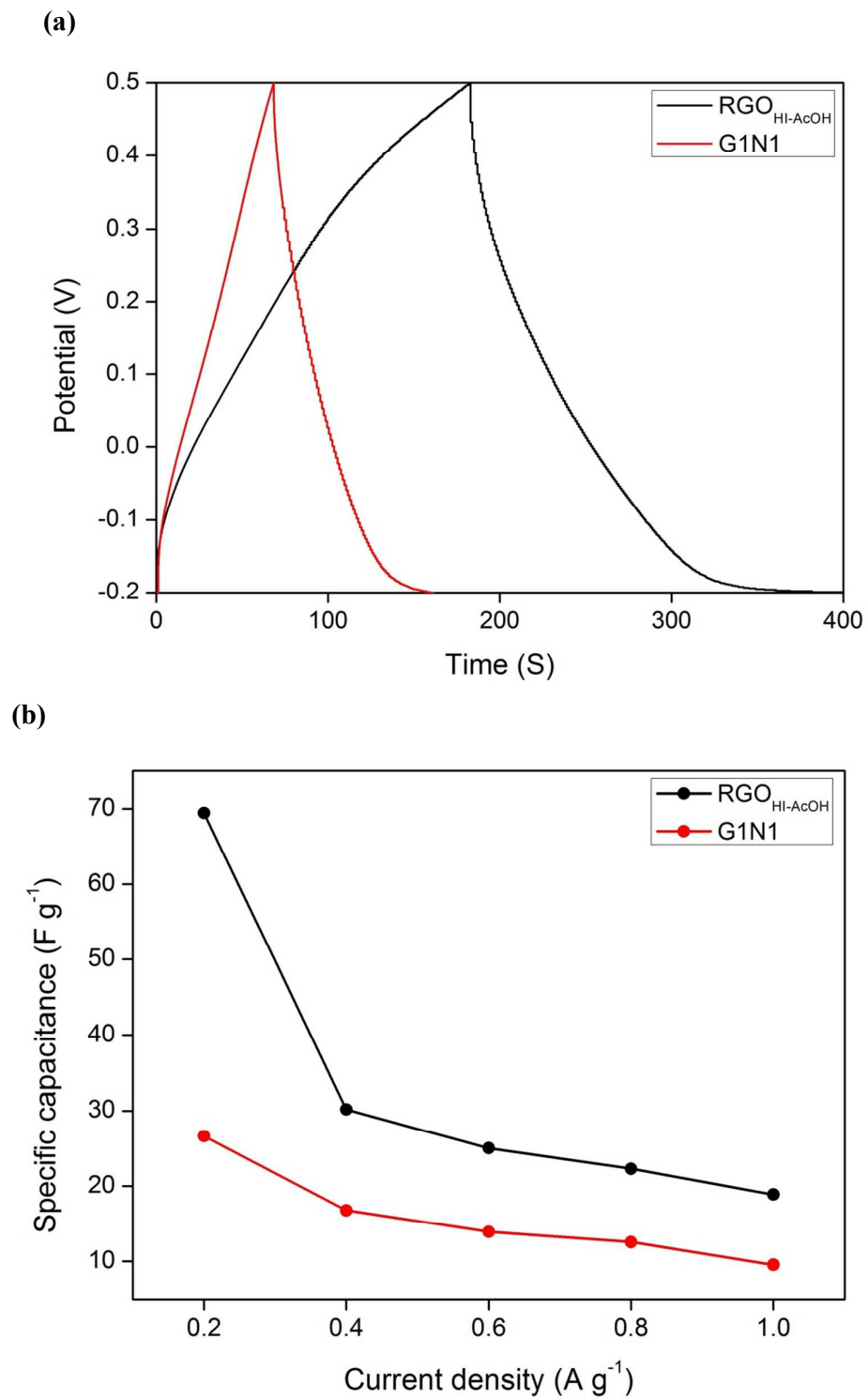


Fig. 9

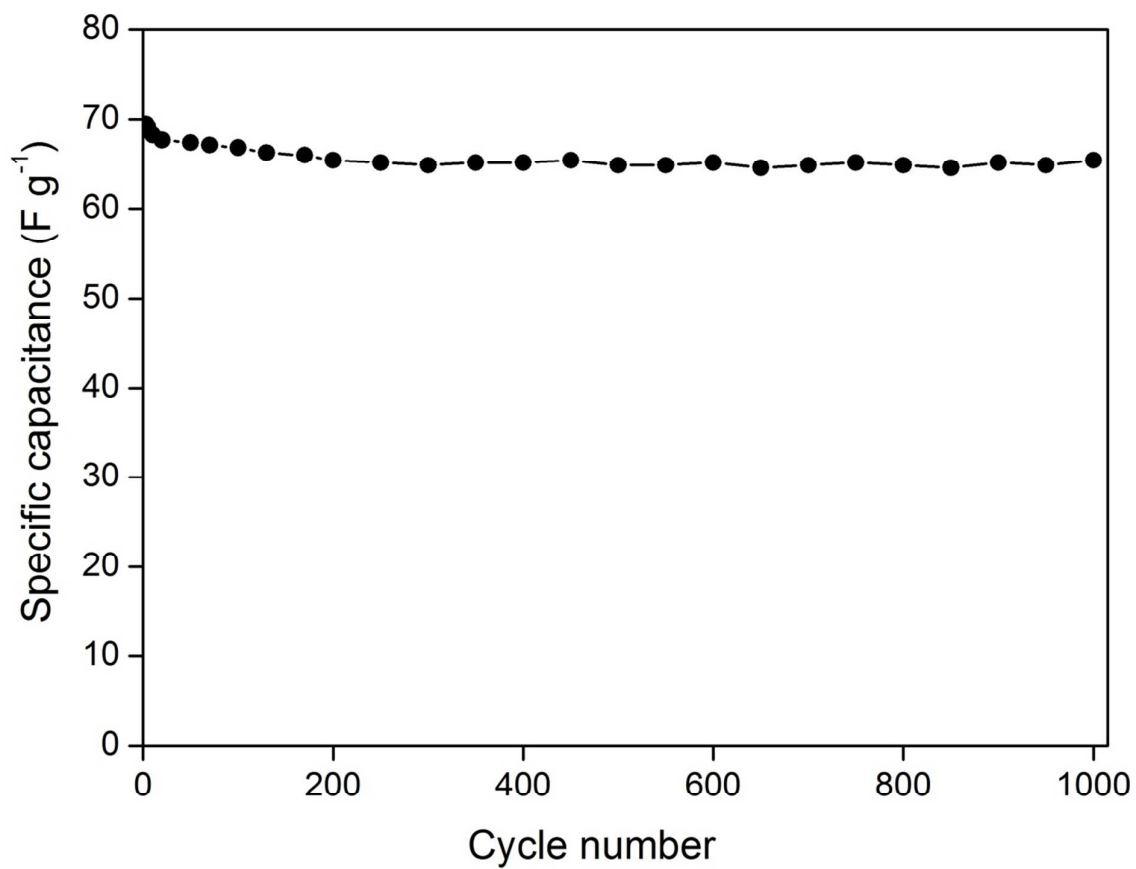


Table 1 Position values of D, G, and 2D bands for the different carbonaceous materials in Raman spectra.

Material	D (cm <sup>-1</sup> )	G (cm <sup>-1</sup> )	2D (cm <sup>-1</sup> )	I <sub>D</sub> /I <sub>G</sub>
GO	1360.06	1596.24	2520.96	0.89
RGO <sub>HI-AcOH</sub>	1346.42	1585.66	2664.92	1.20
RGO <sub>hydrazine</sub>	1346.42	1593.60	2682.96	1.08
G1N1	1349.15	1593.60	2960.66	0.98